Mt. Etna tropospheric ash retrieval and sensitivity analysis using Moderate Resolution Imaging Spectroradiometer measurements

Stefano Corradini[a], Claudia Spinetti[a], Elisa Carboni[b], Cecilia Tirelli[c], Maria F. Buongiorno[a], Sergio Pugnaghi[d], and Gabriele Gangale[d]

[a] Istituto Nazionale di Geofisica e Vulcanologia, Via di Vigna Murata 605, 00143 Roma, Italy
corradini@ingv.it, spinetti@ingv.it, buongiorno@ingv.it

[b] Atmospheric Oceanic and Planetary Physics, Clarendon Laboratory, University of Oxford, Parks Road Oxford OX1 3PU, U.K.
elisa@atm.ox.ac.uk

[c] Dipartimento di Fisica, Universitá degli Studi di Roma "La Sapienza", Piazzale Aldo Moro 5, 00185 Roma, Italy
tirelli@g24ux.phys.uniroma1.it

[d] Dipartimento di Ingegneria Materiali e Ambiente, Universitá di Modena e Reggio Emilia, Via Vignolese 905, 41100 Modena, Italy
sergio.pugnaghi@unimore.it, gabriele.gangale@unimore.it

Abstract. A retrieval of tropospheric volcanic ash from Mt Etna has been carried out, using measurements from the Moderate Resolution Imaging Spectroradiometer (MODIS). The NASA-MODIS satellite instrument acquires images in the 0.4 to 14 μm spectral range with a spatial resolution of 1 km at nadir. The eruption which occurred on 24 November 2006 is considered as a test case in this work. In order to derive the ash plume optical thickness, the particle effective radius and the total mass, the Brightness Temperature Difference procedure has been applied to MODIS channels 31 (centered at 11 μm) and 32 (centered at 12 μm). Channel 5 (centered at 1.24 μm) has been used to refine the cloud discrimination, exploiting the distinct reflectivity of meteorological and volcanic clouds in the near infrared spectral range. The detection of volcanic ash pixels has been significantly improved by applying an atmospheric water vapor correction to MODIS data. This procedure doubles the number of pixels identified as containing volcanic ash compared to the original method. The retrieved mean ash optical thickness at 0.55 μm, mean particle effective radius and the total ash mass in the plume are 0.4, 3.5 μm and 3620 tons, respectively. A detailed sensitivity analysis has been carried out to investigate errors in the retrieval caused by the uncertainty in various parameters: surface temperature and emissivity, plume geometry (altitude and thickness), ash type and atmospheric water vapor. Results show that the largest contributions to retrieval errors are from uncertainty in surface parameters, aerosol type and atmospheric water vapor. The total tropospheric volcanic ash retrieval errors are estimated to be 30%, 30% and 40% for mean AOT, mean effective radius and total mass retrieval, respectively.

Keywords: volcanic ash, Mt. Etna volcano, MODIS, sensitivity study, MODTRAN radiative transfer model.

1 INTRODUCTION

Volcanic eruptions inject huge amounts of solid particles [1] into the atmosphere. Volcanic ash is composed of fragments of pyroclast rocks smaller than 2 mm which are released during explosive events, forming the typical volcanic plume and leading to characteristic ash falls [2]. Depending on eruptive intensity the volcanic ash can reach different altitudes in the atmosphere.

Received 20 Dec 2007; accepted 18 Nov 2008; published 21 Nov 2008 [CCC: 19313195/2008/$25.00]

Residence time depends on particle size [3]. Ash particles with radius greater than 100 μm may have a very short residence time from minutes to less than an hour, while ash particles with radius lower than 10 μm can travel hundreds to thousands of kilometers downwind from the volcano remaining suspended in the atmosphere for hours to weeks. Volcanic ash falls cause respiratory problems [4], damage to agricultural and industrial activities [5] and problems for terrestrial and air transport [4–6]. In particular, volcanic ash clouds are a severe threat to aviation security [7]. Particles with dimension of several millimeters can damage the aircraft structure (windows, wings, ailerons), while particles less than 10 μm may be extremely dangerous for the jet engine and undetectable by the pilots during night or in low visibility conditions [8]. Volcanic fine ash clouds can not be detected by aircraft radar and they are often indistinguishable from water clouds even in daytime. For these reasons several methodologies and algorithms have been developed and tested in order to detect and track drifting volcanic ash clouds either in the Thermal InfraRed (TIR) and/or the UltraViolet (UV) spectral range. Theoretical calculation demonstrates that in the TIR 10-13 μm spectral range, the radiative effect of volcanic ash clouds is spectrally distinct from that of water droplets [9, 10]. In particular the difference between the brightness temperature of two channels centered around 11 μm and 12 μm, is used to discriminate volcanic and meteorological clouds and for volcanic ash retrievals [11–13]. The TIR spectral range is sensitive to coarse ash particles, while the UV spectral range is also sensitive to fine particles [14, 15].

Because of the sporadic nature of volcanic eruptions, the large geographic distribution of volcanoes and the difficulty of direct sampling, remote sensing provides the most suitable technique to detect and retrieve volcanic emissions on a consistent and comprehensive basis. The retrieval and discrimination between cloud and volcanic ash has been performed using various satellite instruments such as the Advanced Very High Resolution Radiometer (AVHRR) [9, 11, 13, 15–18], Geostationary Operational Environmental Satellite (GOES) [13, 19, 20], Total Ozone Mapping Spectrometer (TOMS) [15, 17] and the Moderate Resolution Imaging Spectroradiometer (MODIS) [20–23].

Mt. Etna, located in the eastern part of Sicily (Italy), is the biggest European volcano and one of the most active volcanoes on the Earth. It's frequent ash emissions cause problems for the local population and in particular for air traffic because of the proximity to airports at Catania and Reggio Calabria.

In this work the retrieval of tropospheric volcanic ash optical thickness (AOT) at 0.55 μm, particle effective radius (r_e) and total mass from MODIS TIR measurements has been studied, using the image of Etna acquired by MODIS on 24 November 2006 as a test case. The cloud discrimination and the volcanic ash retrievals have been carried out using the Brightness Temperature Difference (BTD) procedure [9–11, 13, 19] applied to MODIS channels 31 and 32 centered at 11 and 12 μm, respectively. Channel 5 (centered at 1.24μm) is used to refine the clouds discrimination algorithm, exploiting the distinct shortwave reflectivity of meteorological and volcanic clouds. To improve the volcanic ash detection and retrieval, an atmospheric water vapor correction has also been developed and applied to the measurements. Both the ash retrieval and the sensitivity study have been carried out using the MODTRAN Radiative Transfer Model (RTM) [24, 25]. The sensitivity analysis has been performed to estimate the ash retrieval error due to the uncertainties on surface temperature and emissivity, plume altitude and thickness, ash optical properties and atmospheric water vapor.

The paper is organized as follows: In Sections 2 the MODIS instrument and test case are described. The cloud discrimination and ash retrieval are presented in Section 3 and in Sections 4 the volcanic ash sensitivity analysis is shown. Section 5 details the conclusions of the study.

2 MODERATE RESOLUTION IMAGING SPECTRORADIOMETER

MODIS is a multispectral instrument on board Terra and Aqua polar satellites, part of the Earth Observing System (EOS) mission [26, 27]. Terra's descending node (from north to south)

crosses the equator in the morning at about 10:30 a.m., while the Aqua ascending node (south to north) crosses the equator at about 1:30 p.m. MODIS acquires data in 36 spectral bands in the wavelength range from visible to thermal infrared. The spatial resolution is 250 m for bands 1 and 2, 500 m for bands 3 to 7 and 1000 m for all other bands. Bands 31 and 32 are centered around 11 and 12 μm respectively with a Noise Equivalent Temperature Difference (NEDeltaT) of only 0.05 K [27]; these two channels are used here both for the discrimination of cloud and the volcanic ash retrieval. Band 5, centered at 1.24μm with a Signal to Noise Ratio of 75 (considering a signal level of 5.4 W/m^2/sr/μm) [27], is used to improve the cloud discrimination. The sensor scans $\pm$55 degree across-track about the nadir from the EOS orbit altitude of 705 km, resulting in a 2330 km swath and full global coverage every one to two days.

2.1 TEST CASE

Mt. Etna is located in the eastern part of Sicily (Italy) and is one the major degassing volcanoes in the world [28]. Its generally quiescent state is periodically interrupted by eruptive periods when significant ash emissions reach areas surrounding the volcano causing problems to the population of the region [29] and to air traffic (Catania and Reggio Calabria airports are nearby).

During 2006 Mt. Etna exhibited episodic explosive activity producing ash plumes that rose up into the atmosphere and drifted several kilometers away from the vent. These episodes occurred frequently from September to December [30, 31] showing weak intensity and short duration compared to previous 2001 and 2002 eruptions [29, 32]. The 24 November 2006 ash emission started at about 03:00 UTC and ended at about 17:00 UTC; this took place at the SE crater located in the southern flank of Mt. Etna and produced the largest volume of ash in the entire September-December eruptive period [33]. On this day the wind was blowing from the N-NW direction. A change in wind direction caused the ash plume to move towards the city of Catania. The ash fallout created major problems for the "Fontanarossa" International Airport of Catania which was subsequently closed to air traffic. The finest portion of ash traveled more than 80 km from the summit craters. The episode was observed at 12:20 UTC on 24 November by MODIS on the Aqua satellite (see Fig. 1), and this scene is considered here as a test case.

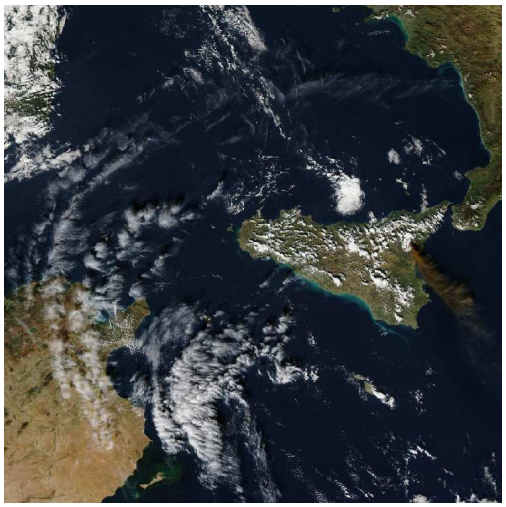

Fig. 1. MODIS-Aqua RGB image acquired on 24 November 2006 at 12:20 UTC.

3 VOLCANIC ASH DETECTION AND RETRIEVAL

In this Section the discrimination between volcanic and meteorological clouds and the ash retrieval is described. To improve the volcanic ash detection and retrievals, an atmospheric water vapor correction procedure has been developed and applied to MODIS measurements.

3.1 Clouds discrimination

The meteorological and volcanic cloud discrimination algorithm is based on the difference between the brightness temperatures observed in two channels centered around 11 and 12 μm. Because of the different spectral optical properties of volcanic and meteorological clouds in the 10-13 μm spectral range, the BTD between the two channels will generally be negative for volcanic clouds (larger absorption at 11 than 12 μm) and positive for meteorological clouds (larger absorption at 12 than 11 μm) [9, 10]. Using the MODIS channels 31 and 32, this BTD has been computed for the test image and Fig. 2 shows the result: The red pixels indicate the volcanic ash (BTD<-0.2 °C) while the blue pixels indicate the meteorological clouds (BTD>1.2 °C). In case of plumes confined to the troposphere, the BTD algorithm gives general good results,

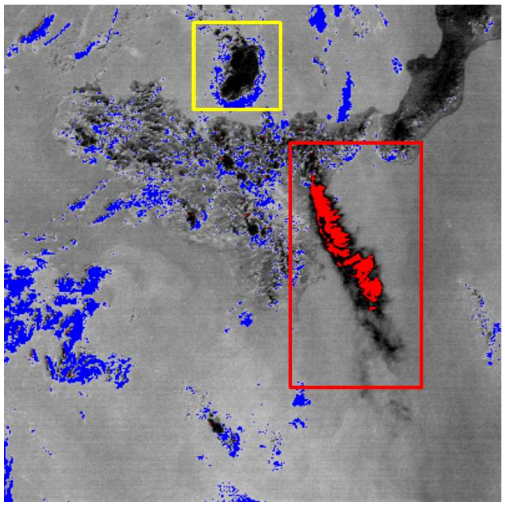

Fig. 2. Cloud detection map using BTD technique. The red color indicates the detected volcanic cloud (BTD<-0.2 °C) and blue the meteorological clouds (BTD>1.2 °C). The yellow and red boxes emphasize that not all meteorological and ash cloud pixels can be unambiguously detected by the procedure.

however not all meteorological clouds are identified (see yellow box in Fig. 2) and not all ash pixels are detected (see red box in Fig. 2).

The cloud discrimination has been improved using the MODIS channel 5 centered around 1.24 μm exploiting the relatively high meteorological cloud reflectivity compared to that of volcanic ash at this wavelength. At this wavelength the real part of the refractive index of the two clouds is comparable (respectively 1.3 and 1.5) while the imaginary part of the meteorological cloud refractive index is much lower that of ash (respectively $4{\cdot}10^{-5}$ and $8{\cdot}10^{-2}$) i.e. the ash cloud absorption at this wavelength is much higher than the meteo cloud absorption. Fig. 3A emphasizes (in yellow) pixels having a Top Of Atmosphere (TOA) reflectance greater than 0.15. Fig. 3B shows the cloud discrimination combining the BTD and channel 5 thresholds.

Fig. 2 and 3B show that, many volcanic ash pixels cannot be detected. The incomplete ash detection is mainly due to the radiative effect of atmospheric water vapor which, in case

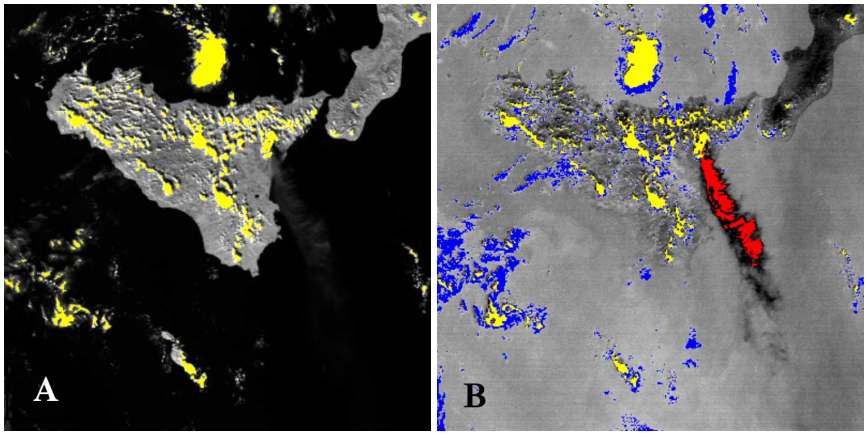

Fig. 3. A: meteorological cloud detection using MODIS channel 5 (in yellow the pixels with TOA > 0.5). B: volcanic and meteorological clouds discrimination using BTD procedure and MODIS channel 5.

of high water vapor or low ash concentrations, can counteracts the radiative effect of volcanic ash [12, 13] in the 11 and 12 μm channels.

3.2 Atmospheric water vapor correction

Absorption by atmospheric water vapor is larger at 12 μm than at 11 μm. The opposite is usually true for volcanic ash and so water vapor absorption can reduce the BTD signal of ash. In case of high columnar content, water vapor can completely cancel-out the ash plume effect on the BTD. For this reason in moist tropical conditions only the densest cores of volcanic clouds can be detected [34]. Prata et al. [12] and Yu et al. [13] proposed a method to correct the water vapor effect using MODTRAN and the global NCEP analysis for four different days and two different times representatives of seasonal and diurnal variation of water vapor. They proposed a nonlinear relation between BTD and brightness temperature at 11 μm for different values of water vapor and applied it to AVHRR and GOES measurements. In this work, a similar procedure, based on MODTRAN simulations and local atmospheric data, has been developed and applied to MODIS measurements.

The procedure is based on the evaluation of the atmospheric water vapor radiative effect on BTD (BTD^w) and on the channel 31 brightness temperature ($\Delta T^w_{b,31}$). BTD^w is used to improve the ash detection (see below), while both BTD^w and $\Delta T^w_{b,31}$ are used for the ash retrieval (see Section 3.3). To evaluate the water vapor radiative effect, two MODTRAN simulations, with and without precipitable water in a clean atmosphere (no ash), have to be carried out. BTD^w is the difference between the brightness temperature of the channels at 11 and 12 μm using the MODTRAN simulation with atmospheric water vapor, while $\Delta T^w_{b,31}$ is the difference between the brightness temperature of channel 31 considering the simulations with and without water vapor.

The sea surface temperature, needed for the computation, has been retrieved using the Split Window (SW) algorithm [35–37] applied to MODIS channels 31 and 32. The SW algorithm, for surface temperature retrieval, needs as input the SW parameters and the emissivity for the two channels. The SW parameters have been computed using the atmospheric correction terms (path radiance, downwelling radiance and transmittance) performed by MODTRAN, using the 24 November 2006 at 12:00 UTC atmospheric vertical profiles measured at Trapani WMO Meteo station (the nearest WMO station to the Etnean area). The sea surface emissivity has been assumed to be the same for both channels and equal to 0.99. Fig. 4A shows the surface

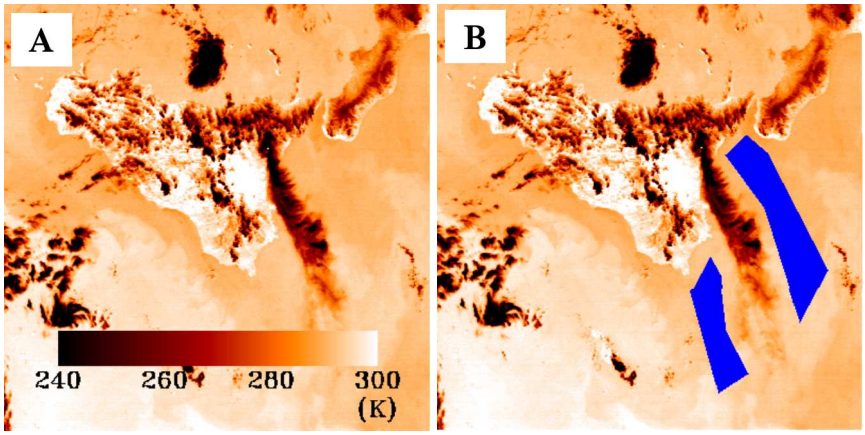

Fig. 4. A: surface temperature map using Split Window technique. B: surface temperature map; in blue the regions selected to associate a sea surface temperature to the region under the plume.

temperature map obtained from this SW algorithm. The retrieved terrestrial surface temperature must be considered only as indicative because of the emissivity values set are representative only for sea surface. Since the volcanic plume is not transparent in channels 31 and 32, the estimation of the surface temperature under the plume from these channels is not possible. The sea surface temperature associated to this region is estimated as the mean temperature of two relatively large regions just outside the plume itself (see blue areas in Fig. 4B). The mean sea surface temperature computed results 292.0 K with a standard deviation of 0.5 K. The low value of the standard deviation indicates that the assumption of considering the sea temperature is constant under the plume is reasonable.

Using the computed sea surface temperature the MODTRAN simulations have been carried out. The water vapor effect is estimated to be 0.6 K and 1.5 K for BTD and $\Delta T_{b,31}$, respectively. The corrected MODIS BTD (BTD*) and $T_{b,31}$ ($T^*_{b,31}$) are obtained using the following equations:

$$BTD^* = BTD - BTD^w \tag{1}$$

$$T^*_{b,31} = T_{b,31} + \Delta T^w_{b,31} \tag{2}$$

Fig. 5 shows the BTD procedure for the ash plume detection before (Fig. 5A) and after (Fig. 5B) the water vapor correction. In Figure 5B the ash pixels have been detected using the same identification criteria used in Figure 5A (i.e. BTD<-0.2). Introducing the water vapor correction, the number of detected ash pixels become more than doubles from 1292 (Fig. 5A) to 3069 (Fig. 5B).

3.3 Volcanic ash retrieval

The particle effective radius, AOT at 0.55 μm and total mass retrievals have been performed by computing, with the MODTRAN RTM, the bell-shaped curves BTD vs. $T_{b,31}$ varying the AOT and the particle's effective radius. [11, 13, 20]. The simulations take as input the atmospheric profiles (pressure, temperature), the plume geometry (plume altitude and thickness), the surface characteristics (temperature and emissivity) and the volcanic ash optical properties. MODIS measurements which have been corrected for atmospheric water vapor absorption, as described in the previous section are used. Therefore the simulations described henceforth are carried out without further consideration of atmospheric water vapor.

As previously described, the 24 November 2006 atmospheric profile was derived from the Trapani WMO Meteo station, while the surface temperature and emissivity have been set to

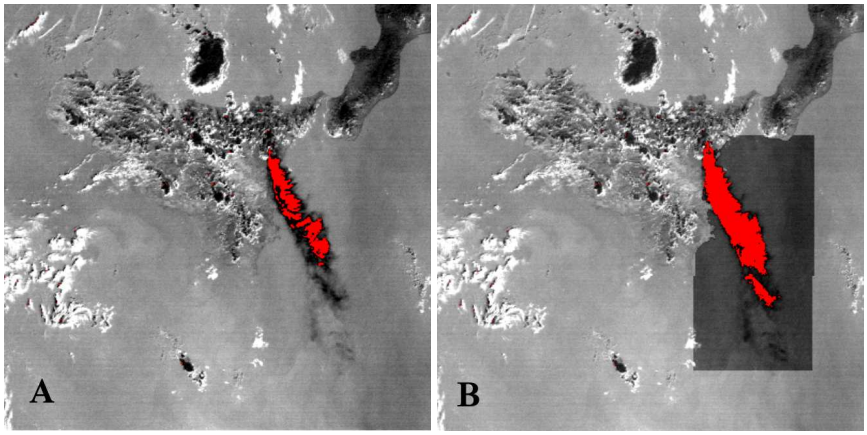

Fig. 5. A: Ash plume detection before water vapor correction. B: Ash plume detection after water vapor correction.

T_s=292 K and e=0.99, respectively (see Section 3.2). The Top Plume Altitude (TPA) has been derived by comparing the ash plume top temperature, computed as mean brightness temperature of channels 31 ($T_{b,31}$) and 32 ($T_{b,32}$) of the most opaque plume region (near the vent), and the Trapani radiosounding temperature profile. The procedure yelds a TPA of about 5000 m consistent with independent observations [30]. The Plume Thickness (PT) has been assumed to be 1000 m.

The ash optical properties (single scattering albedo, extinction coefficient and asymmetry parameter) have been computed using the Mie code developed by the Earth Observation Data Group (EODG) of the Atmospheric Oceanic and Planetary Physics Department (Oxford University) [38] considering the volcanic ash refractive index tabulated by Volz [39] and a log-normal distribution (width (σ)=1.77, minimal and maximal radii corresponding to +/-3σ from the central wavelength). The optical properties have been computed for 10 different particle effective radii ranging from 0.4 to 10 μm with fixed intervals in the logarithm of the effective radius. Fig. 6 shows the Volz real and imaginary part of the ash refractive index and the optical properties (extinction efficiency factor, single scattering albedo and asymmetry parameter) derived from the Mie code, for different effective radii. For each particle effective radius the MODTRAN simulations have been carried out considering 21 values of AOT (from 0 to 10 step 0.5).

Fig. 7 shows the BTD vs. $T_{b,31}$ curves considering all AOT values and effective radius ranging from 1.13 to 10 μm; the near horizontal solid lines represent different effective radii and the near vertical dashed lines represent different AOT. The superimposed red crosses are the ash pixel values detected in the MODIS image after water vapor correction on BTD (see Fig. 5B) and $T_{b,31}$ (see Section 3.2). Below 1 μm all curves superimpose, so 1 μm represents the lower effective radius retrieval detection limit. The upper effective radius detection limit is about 7 μm because for greater values the BTD becomes positive, i.e. the volcanic ash clouds are not distinguishable from meteorological clouds. Analyzing the bell-shaped curve it can also be noted that the BTD values are, in general, significantly lower than the BTD obtained considering stratospheric plumes [11, 13] because of the lower thermal contrast between the tropospheric plume and surface. The convergence point at the right-hand side (AOT=0) is characterized by 0 BTD and $T_{b,31}$ $\cong$292 K because no atmospheric water vapor has been included in the simulations and because the only radiation source is the sea surface. The $T_{b,31}$ left-hand side convergence point represents the brightness temperature of the thick core plume i.e. approximately the temperature of the volcanic plume top. Fig. 8 shows the histogram of AOT and effective radii; the mean AOT ($\overline{AOT}$) is 0.42 and the mean particle effective radius ($\overline{r_e}$) is 3.44

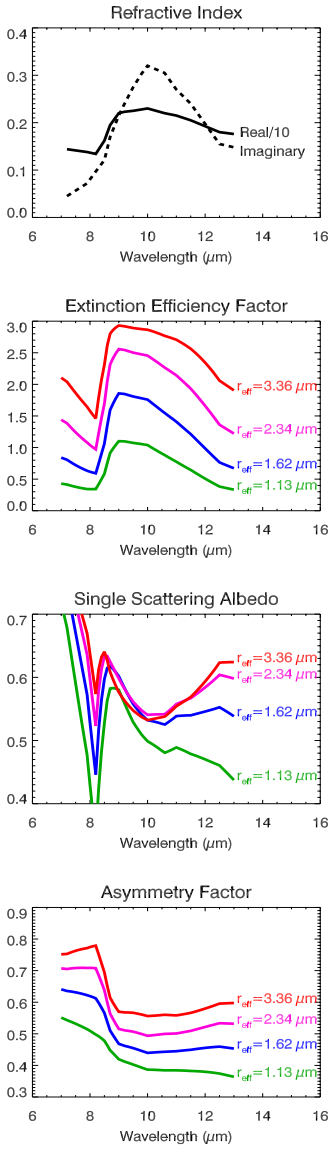

Fig. 6. From top to bottom: Real and imaginary parts of the volcanic ash refractive index considered [39]; extinction efficiency factor; single scattering albedo; asymmetry factor. All the ash optical properties have been computed by the Mie code considering different particle effective radii (1.13, 1.62, 2.34, 3.36 μm).

μm.

The volcanic ash total mass have been computed using the equation suggested by Wen and Rose [11], based on the assumption of uniform particle distribution, and using a particle density

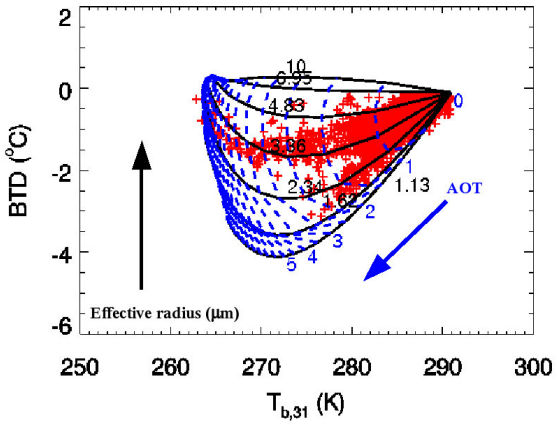

Fig. 7. BTD vs. $T_{b,31}$ curves considering T_s=292 K, a plume top altitude of 5000 m and geometric thickness of 1000 m. The near horizontal solid curves represent different effective radii and the near vertical dashed curves represent different AOT at 0.55 μm. The red crosses are the volcanic ash pixel values revealed on MODIS image after the water vapor correction on both BTD and $T_{b,31}$.

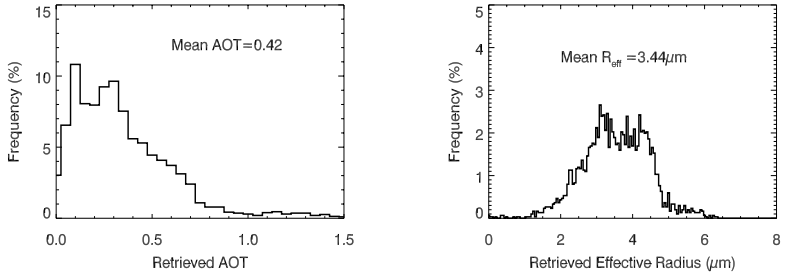

Fig. 8. A: Retrieved AOT at 0.55 μm histogram. B: retrieved effective radius histogram.

of 1.3 g cm^{-3} (Coltelli private communication):

$$M_{tot} = \frac{S4/3\rho {r_e}^{(n,m)} \tau^{(n,m)}}{Q_{ext}(r_e^{(n,m)})} \tag{3}$$

where: S is the pixel surface; ρ is the particle density; $r_e^{(n,m)}$ is the effective radius of pixel (n,m); $\tau(n,m)$ is the AOT of pixel (n,m); $Q_{ext}(r_e^{(n,m)})$ is the extinction efficiency factor at effective radius $r_e^{(n,m)}$. Fig. 9 shows maps of the retrieved volcanic ash plume AOT, particle effective radius and mass. As expected, the largest AOT occurs in the area close to the vent and the smallest at the cloud edges. There are also other regions of high AOT probably due to volcanic puffs. The particle effective radii are distributed non-uniformly along the plume: the larger particles (up to 3.5 μm) are found around the western part of the plume itself. The computation of total plume ash mass gives 3620 tons.

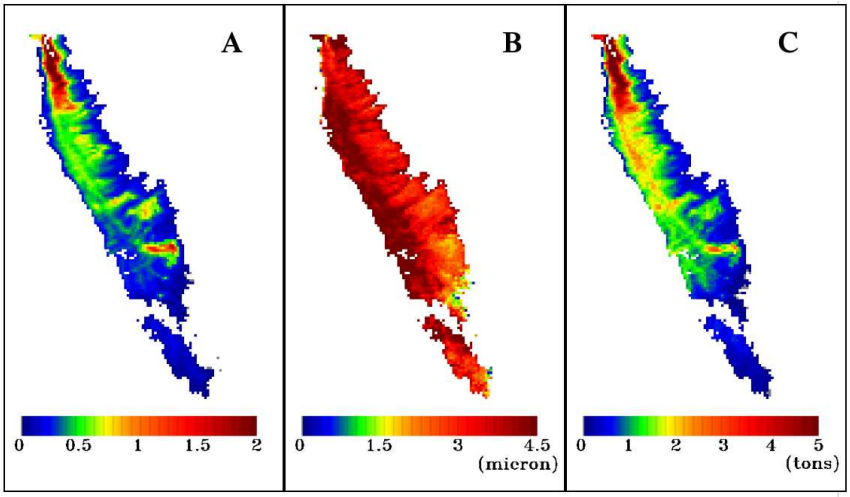

Fig. 9. A: 0.55 μm AOT plume retrieval map. B: effective radius plume retrieval map. C: plume total mass map.

4 SENSITIVITY ANALYSIS

The aim of the sensitivity analysis is to compute the volcanic ash retrieval errors due to the uncertainties in parameters input to the MODTRAN simulations: surface characteristics (temperature and emissivity), plume geometry (altitude and thickness), ash optical properties and water vapor columnar content. The results with modified parameters are compared with those obtained assuming the original setting parameters described in the previous Section.

4.1 Surface temperature

The sea surface temperature uncertainty has been set to $\pm$2 K and $\pm$5 K with respect to the retrieved sea surface temperature using SW technique (292 K, see Section 3.2). Therefore MODTRAN simulations have been carried out considering 4 values of surface temperature (287, 290, 294 and 297 K) and preserving all other input parameters. Fig. 10 shows the computed BTD vs. $T_{b,31}$ curves computed; the lower the surface temperature, the tighter the BTD vs. $T_{b,31}$ curves and generally, the lower the retrieved ash amount. In Table 1 the number of ash pixels detected, $\overline{AOT}$, $\overline{r_e}$ and total mass retrievals for the different assumed T_s values and the percentage difference with respect to the original retrievals are summarized. As shown in Table 1, the greatest variations in the total mass retrieval arise because of the significant variation in the number of volcanic ash pixels detected. For example considering T_s=297 K the water vapor BTD correction is approximately doubled (1.1° C) compared to the original water BTD correction (0.6° C). The sea surface temperature overestimation produces an incorrect identification of sea pixels as volcanic ash pixels, that causes a huge overestimation of the total mass retrieved. Moreover the incorrect identification of sea pixels as ash pixels also leads to a large underestimation of the mean AOT, because such values falls near the right-hand convergence point, since their $T_{b,31}$ values are close to T_s. Uncertainty of $\pm$2 K on surface temperature produces small retrieval errors on AOT and effective radius retrievals (always less than 7%) but a large total mass retrieval error of about 30%. Table 1 also shows that for large surface temperature overestimation (+5 K) the ash retrieval errors are larger than in the case of high temperature underestimation (-5 K).

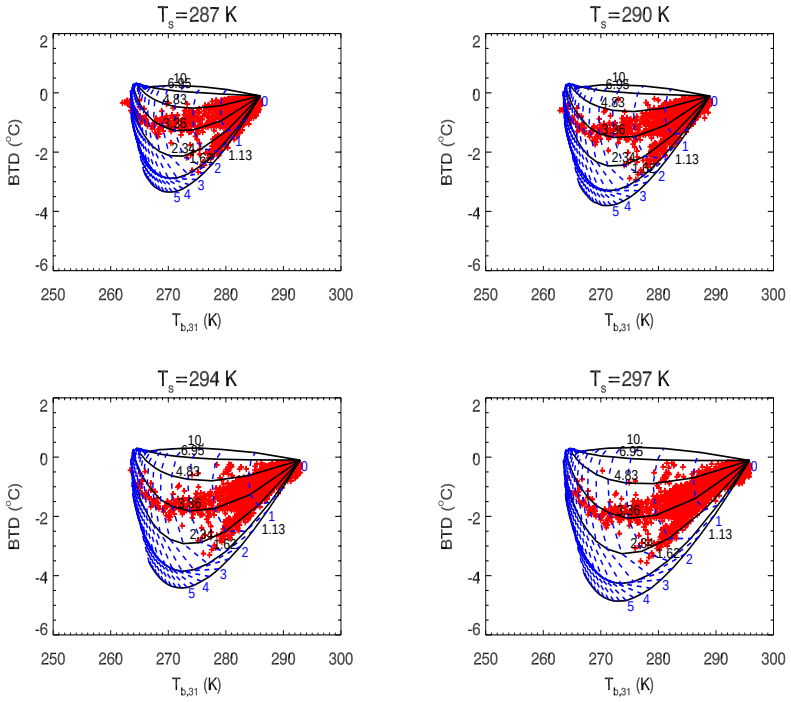

Fig. 10. BTD vs. $T_{b,31}$ curves considering different surface temperatures: 287, 290, 294 and 297 K. The red crosses are the volcanic ash pixel values revealed on MODIS image after the water vapor correction.

Table 1. Total number of ash pixel detected, mean AOT, mean r_e and total mass retrieved considering different surface temperatures. The percentage difference is computed considering the original retrieval.

T_s (K)	N° pixel (var %)	$\overline{AOT}$ (var %)	$\overline{r_e}$ (μm) (var %)	Total mass (tons) (var %)
287	1597 (-48)	0.42 (0)	3.02 (-12)	1907 (-47)
290	2376 (-23)	0.42 (0)	3.33 (-3)	2830 (-22)
294	4429 (28)	0.39 (7)	3.54 (5)	4723 (30)
297	19691 (541)	0.23 (-45)	4.44 (29)	15145 (318)

4.2 Surface emissivity

In this section the ash retrieval errors due to surface emissivity uncertainty are analyzed. In accordance with typical surface emissivity variations in the 11-12 μm spectral range [40], the MODTRAN simulations have been carried out introducing surface emissivity uncertainties of

2 and 5% with respect to the surface emissivity originally set (e=0.99). Fig. 11 shows the BTD vs. $T_{b,31}$ curves computed for e=0.94 and e=0.97. In Table 2 the $\overline{AOT}$, $\overline{r_e}$ and total mass retrievals for the different emissivities considered and the percentage differences with respect to the original retrievals are summarized. The lower the surface emissivity, the lower the number

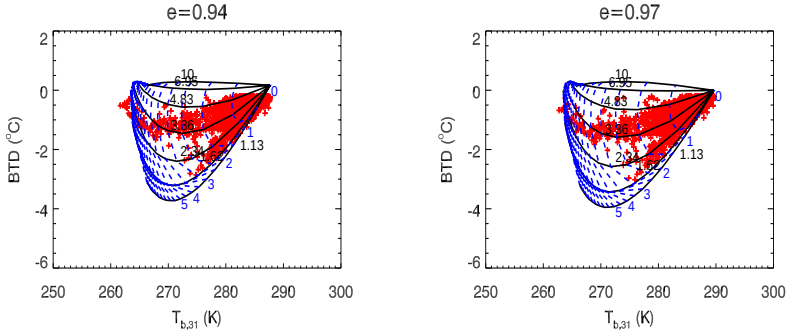

Fig. 11. BTD vs. $T_{b,31}$ curves considering surface emissivity of 0.94 (left) and 0.97 (right). The red crosses are the volcanic ash pixel values from the MODIS image after the water vapor correction.

Table 2. Total number of ash pixels detected, mean AOT, mean r_e and total mass retrieved considering different surface emissivities. The percentage difference is computed relative to the original retrieval.

e	N° pixel (var %)	$\overline{AOT}$ (var %)	$\overline{r_e}$ (μm) (var %)	Total mass (tons) (var %)
0.94	2166 (-30)	0.52 (24)	2.99 (-17)	2943 (-19)
0.97	2660 (-13)	0.46 (9)	3.25 (-7)	3309 (-9)

of detected pixels , because the water vapor correction is now less important than in the original case. An uncertainty of $\pm 2\%$ on surface emissivity produces significant retrieval errors on AOT, r_e and total mass, of about 10%.

4.3 Plume geometry and altitude

The plume geometry and altitude sensitivity is computed varying the plume-top altitude and the plume geometric thickness. In the original simulations the plume top has been placed at 5000 m with thickness of 1000 m. The sensitivity is assessed varying the Plume-top Altitude (TPA) to 4500 and 5500 m maintaining constant the Plume Thickness (PT) (1000 m), and varying the plume thickness at 500 m maintaining constant the plume-top altitude (5000 m). Fig. 12 shows the BTD vs. $T_{b,31}$ curves relative to the simulations described. As expected the curves are dilated for a plume placed at higher altitudes because the greater thermal contrast between surface and plume. Table 3 summarizes the $\overline{AOT}$, $\overline{r_e}$ and total mass retrievals for the different plume geometries and the percentage difference relative to the original retrievals. The uncertainties on plume altitude and thickness produce retrieval errors of about 10% for AOT and total mass and less then 5% for effective radius.

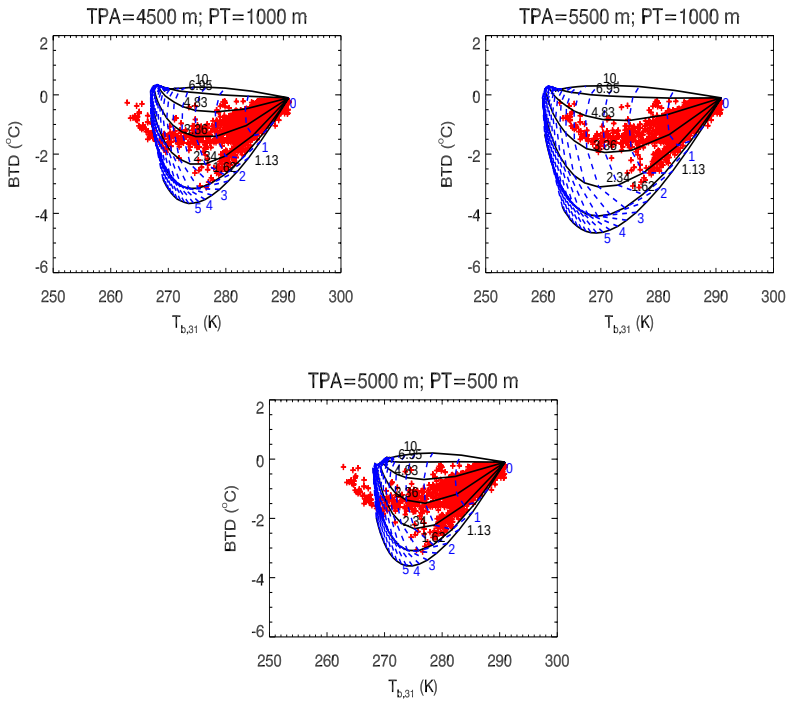

Fig. 12. BTD vs. $T_{b,31}$ curves varying the plume geometry. The red crosses are the volcanic ash pixel values from the MODIS image after the water vapor correction. Top left: top plume altitude = 4500 m, plume thickness = 1000 m. Top right: plume-top altitude = 5500 m, plume thickness = 1000 m. Bottom: plume altitude = 5000 m, plume thickness = 500 m.

Table 3. Total number of ash pixel detected, mean AOT, mean r_e and total mass retrieved considering different geometries. The percentage difference is computed relative to the original retrieval.

Plume Geometry	N° pixel (var %)	$\overline{AOT}$ (var %)	$\overline{r_e}$ (μm) (var %)	Total mass (tons) (var %)
TPL=4.5 km	3069 (0)	0.46 (9)	3.36 (-4)	3733 (3)
TPL=5.5 km	3069 (0)	0.37 (-12)	3.62 (4)	3369 (-7)
PT=0.5 km	3069 (0)	0.39 (-7)	3.45 (-1)	3255 (-10)

4.4 Aerosol type

In this section the sensitivity analysis is performed using a different aerosol type. In a new retrieval the andesite refractive index has been extracted from Pollack et al [41]. Fig. 13 compares the imaginary part of the refractive index of andesite and that of volcanic ash (from Volz) which was used for all the previous simulations. Also plotted in Fig. 13 the spectral response functions of MODIS channels 31 and 32; as figure shows, in the 10-12 μm spectral range, the Andesite

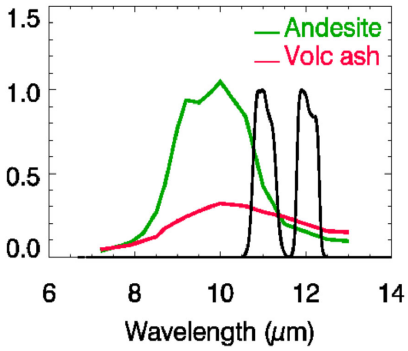

Fig. 13. Imaginary part of the Refractive index of volcanic ash tabulated by Volz and Andesite tabulated by Pollack. The black curves are the MODIS-Aqua channels 31 and 32 spectral response functions.

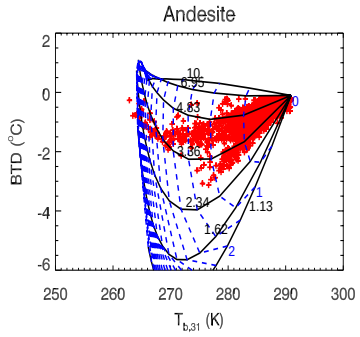

Fig. 14. Bell-shaped curve for Andesite aerosol. The red crosses are the volcanic ash pixel values from the MODIS image after the water vapor correction.

imaginary refractive index is more skewed than that of volcanic ash. The optical properties (extinction efficiency factors, single scattering albedo and asymmetry parameters), needed for MODTRAN simulations, have been computed using the Mie code with the Andesite refractive index. In Fig. 14 the BTD vs. $T_{b,31}$ curves for the Andesite aerosol type are shown. The Andesite curves are more dilated than volcanic ash curves but the effective radius detection limit is about the same (7 μm). The results shown in Table 4 show a significant overestimation for both r_e and total mass (about 20%).

Table 4. Total number of ash pixels detected, mean AOT, mean r_e and total mass retrieved considering Andesite optical properties. The percentage difference is computed relative to the original retrieval.

Aerosol type	N° pixel (var %)	$\overline{AOT}$ (var %)	$\overline{r_e}$ (μm) (var %)	Total mass (tons) (var %)
Andesite	3169 (0)	0.41 (-2)	4.19 (20)	4232 (17)

4.5 Atmospheric Water vapor

As described in Section 3.2 the water vapor correction has been carried out by means of MODTRAN simulations using as input the Trapani Meteo station atmospheric water vapor profile. Given that the distance between Trapani and Etna (about 250 km) could lead to significant differences in atmospheric water vapor between the two locations, a sensitivity study has been carried out to estimate the corresponding ash retrieval errors. From the analysis of 14 years (from 1989 to 2003) of Trapani Meteo Station atmospheric radio-soundings, a variability of 30% in water vapor profile in November has been estimated [42]. The spatial water vapor columnar abundance variability has been set to $\pm 10\%$ and $\pm 20\%$ of the reference 24 November at 12:00 UTC Trapani atmospheric profile. In Fig. 15 the BTD vs. $T_{b,31}$ curves for the different water vapor columnar abundances considered are shown. As Table 5 shows the AOT, r_e and

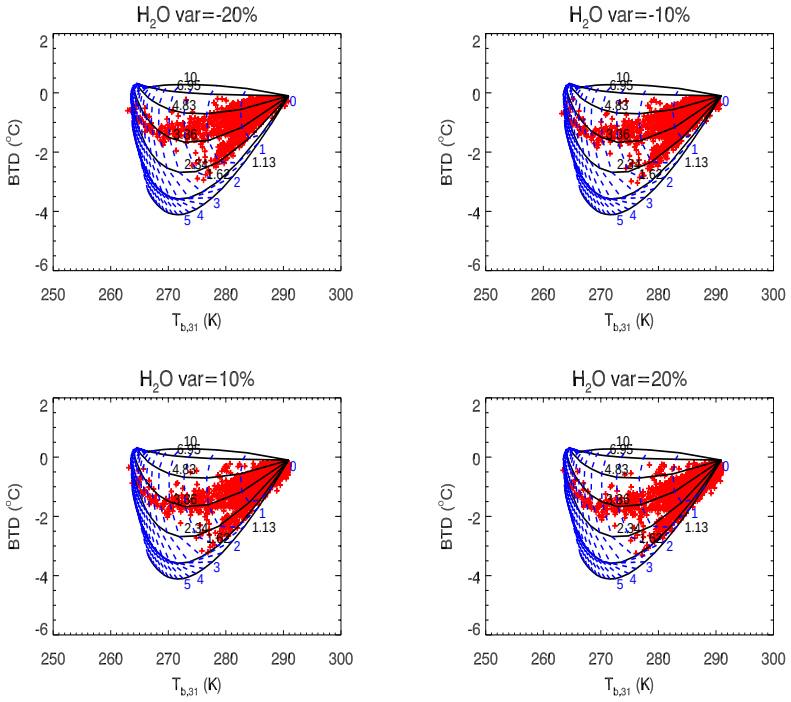

Fig. 15. Bell-shaped curves considering different atmospheric water vapor amounts. The red crosses are the volcanic ash pixel values from the re MODIS image after the water vapor correction.

total mass retrieval errors are approximately proportional to the water vapor uncertainty i.e. a 10% or 20% of water vapor columnar abundance variability produces retrieval errors of about 10% and 20% respectively. This indicates that the atmospheric water vapor columnar content uncertainty represents one of the larger sources of volcanic ash retrieval errors.

4.6 Total retrieval error

From the error propagation theory, assuming errors are independent of each other, the total retrieval error (E_{tot}) is given by the square root of the square error sum:

$$E_{tot} = \sqrt{(E_{T_s})^2 + (E_\epsilon)^2 + (E_{TPA})^2 + (E_{PT})^2 + (E_{type})^2 + (E_{wv})^2} \qquad (4)$$

Table 5. Total number of ash pixels detected, mean AOT, mean r_e and total mass retrieved considering different atmospheric water vapor amounts. The percentage difference is computed relative to the original retrieval.

H_2O % var	N° pixel (var %)	$\overline{AOT}$ (var %)	$\overline{r_e}$ (μm) (var %)	Total mass (tons) (var %)
-20	2433 (-22)	0.51 (21)	4.20 (20)	4000 (10)
-10	2743 (-12)	0.47 (12)	3.89 (11)	3833 (6)
10	3422 (10)	0.38 (-10)	2.96 (-15)	3283 (-9)
20	3601 (16)	0.35 (-17)	2.34 (-33)	2890 (-20)

where E_{T_s}, E_ϵ, E_{TPA}, E_{PT}, E_{type} and E_{wv} are the surface temperature, surface emissivity, plume-top altitude, plume thickness, aerosol optical properties and water vapor retrieval errors, respectively. Considering a surface temperature, emissivity and water vapor columnar abundance uncertainty of 2 K, 2% and 20% respectively, the total percentage retrieval errors are summarized in Table 6. Table 6 also shows also the volcanic ash retrieval errors, neglecting the water vapor uncertainty i.e. assuming the correct atmospheric water vapor profile is known. These results indicate that the knowledge of a precise water vapor atmospheric profile signifi-

Table 6. Total percentage retrieval errors for mean AOT, mean r_e and total mass. The last column indicates the retrieval errors neglecting the water vapor uncertainty.

	Total retrieval error (%)	Total retrieval error (%) (no water vapor error)
AOT mean	30	20
r_e mean (μm)	30	20
Total mass	40	30

cantly reduces the ash retrieval errors.
Considering the estimated total errors, the retrieved volcanic ash quantities can be written as: AOT = 0.4 $\pm$0.1, r_e = 3.5 $\pm$1.1 μm, total mass = 3620 $\pm$1448 tons.

5 CONCLUSIONS

In this work the retrieval of tropospheric volcanic ash from Mt. Etna has been carried out using MODIS measurements, together with a sensitivity study to assess retrieval errors. As a test case the 24 November 2006 Mt. Etna image, acquired at 12:20 UTC, has been considered. The meteorological and volcanic cloud discrimination and the effective radius, AOT and total ash mass retrievals have been carried out using the BTD technique applied to MODIS channels 31 (centered at 11 μm) and 32 (centered at 12 μm). MODIS channel 5 (centered around 1.24 μm) was used to improve the cloud discrimination by exploiting the distinct reflectivity of meteorological and volcanic clouds in the near infrared spectral range. An atmospheric water vapor correction procedure, based on MODTRAN RTM calculations and local measurements, has been applied to improve the volcanic ash detection. The water vapor correction doubles the number of pixels identified as containing volcanic ash compared to the original procedure.

The $\overline{AOT}$, $\overline{r_e}$ and total mass retrievals are obtained by computing the BTD vs. $T_{b,31}$ curves as a function of AOT and effective radius, using MODTRAN. The ash optical properties (single scattering albedo, extinction coefficients and asymmetry parameters) were derived using the EODG-AOPP Mie code assuming volcanic ash refractive indices tabulated by Volz [39] and a log-normal particle size distribution.

Simulations indicate that the effective radius retrieval is possible in the range 1-7 μm. The near horizontal bell-shaped curves for effective radii lower than 1 μm are superimposed on each other, while for effective radii greater than 7 μm the BTD is positive and so ash becomes indistinguishable from water particles radiative effect. The retrieved mean AOT, mean effective radius and total mass are 0.4, 3.5 μm and 3620 tons, respectively. The AOT plume map indicates larger values close to the vent and smaller at the cloud edges; large AOT values also occur in different parts of the plume, due to volcanic puffs. The effective radius plume map indicates a non-uniform distribution of particle size distribution; the largest particles have been observed in the western part of the volcanic plume.

The volcanic ash retrieval sensitivity study has been carried out to estimate the errors due to the uncertainties of different model parameters. Results show that surface parameters (temperature and emissivity) and water vapor uncertainties produce significant errors on all volcanic ash retrievals. Changing the assumed aerosol type led to significant uncertainties on r_e and total mass retrieval while significant retrieval errors on AOT were produced by plume altitude uncertainty. The total retrieval errors have been estimated to be 30%, for both AOT and effective radius and 40% for total mass. Assuming the atmospheric water vapor profile is known i.e. neglecting the water vapor uncertainty, reduces the AOT and effective radius retrieval uncertainties to 20% and total mass at 30%. Finally, results clearly indicate the need to use atmospheric profile measurements which accurately represent the volcanic area.

Acknowledgments

This work was supported by ASI SRV project, MIUR-FIRB B5 Project and by DPC project V3_6-Etna. The data has been provided by Telespazio to INGV under the pre-operative test of Preview Eurorisk project funded by European Community in the FP6 framework.

Authors would like to thank the Atmospheric Oceanic and Planetary Physics Earth Observation Data Group (AOPP-EODG) of the Oxford University for the Mie Code. Authors would further like to thank Dr. Stefano Gagliano (ITT Visual Information Solution) for his software suggestions and Dr. Richard Siddans for carefully reading the original manuscript and for providing helpful comments and language corrections.

This paper is published despite the effects of the Italian law 133/08. This law drastically reduces the resources to public Italian universities and research institutions, which is particularly dangerous for scientific free research, and it will prevent young researchers from getting a position, either temporary or tenured, in Italy. All the authors are protesting against this law to obtain its cancellation.

References

[1] J. P. Kotra, D. L. Finnegan, W. H. Zoller, M. A. Hart, and J. L. Moyers, "El Chichon: composition of llume gases and particles," *Science* **222**, 1018 (1983) [doi:10.1126/science.222.4627.1018].

[2] R. A. F. Cas and J. V. Wright, *Volcanic successions modern and ancient*, Chapman & Hall press (1987).

[3] G. Fiocco, D. Fua, and G. Visconti, "The Mount Pinatubo eruption effects on the atmosphere and climate," *Proc. NATO ASI Series, Series 1: Global Environmental Change* **42** (1984).

[4] C. J. Horwell and P. J. Baxter, "The respiratory health hazards of volcanic ash: a review for volcanic risk mitigation," *Bull. Volcanol.* **69** (1), 1-24 (2006) [doi:10.1007/s00445-006-0052-y].

[5] C. Stewart, D. M. Johnston, G. S. Leonard, C. J. Horwell, T. Thordarson, and S. J. Cronin, "Contamination of water supplies by volcanic ashfall: a literature review and simple impact modelling," *J. Volcanol. Geoth. Res.* **158** (3-4), 296-306 (2006) [doi:10.1016/j.jvolgeores.2006.07.002].

[6] L. Gurioli, M. T. Pareschi, E. Zanella, R. Lanza, E. Deluca, and M. Bisson, "Interaction of pyroclastic density currents with human settlements: Evidence from ancient Pompeii," *Geology* **33** (6), 441444 (2005) [doi:10.1130/G21294.1].

[7] T. J. Casadevall, (ed.), "Volcanic ash and aviation safety," *Proceedings of the First International Symposium on Volcanic Ash and Aviation Safety: U.S. Geol. Surv. Bull.* **2047**, 450 (1994).

[8] G. L. Hufford, L. J. Salinas, J. J. Simpson, and E. G. Barske, & D. C. Pieri, "Operational implications or airborne volcanic ash," *Bull. Am. Meteorol. Soc.* **81** (4), 745755 (2000) [doi:10.1175/1520-0477(2000)081<0745:OIOAVA>2.3.CO;2].

[9] A. J. Prata, "Observation of volcanic ash clouds using AVHRR-2 radiances," *Int. J. Rem. Sens.* **10** (4-5), 751-761 (1989) [doi:10.1080/01431168908903916].

[10] A. J. Prata, "Radiative transfer calculations for volcanic ash clouds," *Geophys. Res. Lett.* **16**(11), 1293-1296 (1989) [doi:10.1029/GL016i011p01293].

[11] S. Wen and W. I. Rose, "Retrieval of sizes and total masses of particles in volcanic clouds using AVHRR bands 4 and 5," *J. Geophys. Res.* **99** (D3), 5421-5431 (1994) [doi:10.1029/93JD03340].

[12] A. J. Prata and I. F. Grant, "Determination of mass loadings and plume heights of volcanic ash clouds from satellite data," *CSIRO Atmosph. Res. Tech. Pap.* **48**, 39, Commonw. Sci. and Ind. res. Organ., Melburne, Victoria, Australia (2001).

[13] T. Yu, W. I. Rose, and A. J. Prata, "Atmospheric correction for satellite-based volcanic ash mapping and retrievals using "split window" IR data from GOES and AVHRR," *J. Geophys. Res.* **107** (D16), 4311 (2002) [doi:10.1029/2001JD000706].

[14] N. A., Krotkov, A. J. Krueger, P. K. Bhartia, "Ultraviolet optical model of volcanic clouds for remote sensing of ash and sulfur dioxide," *J. Geophys. Res.*, **102** (D18), 21891-21904 (1997), [doi:10.1029/97JD01690]

[15] N. A., Krotkov, O. Torres, C. Seftor, A. J. Krueger, A. Kostinski, W. I. Rose, G. J. S. Bluth, D. Schneider, and S. J. Schaefer, "Comparison of TOMS and AVHRR volcanic ash retrievals from the August 1992 eruption of Mt. Spurr," *Geophys. Res. Lett.* **26**(4) 455458 (1999) [doi:10.1029/1998GL900278]

[16] L. E. Holasek and W. I Rose, "Anatomy of 1986 Augustine volcano eruptions as recorded by multispectral image processing of digital AVHRR weather satellite data," *Bull. Volcanol.* **53** 420-435 (1991) [doi:10.1007/BF00258183].

[17] D. J. Shneider, W. I. Rose, L. R. Coke, G. J. S. Bluth, I. Sprod, and A. J. Krueger, "Early evolution of stratospheric volcanic eruption cloud as observed with TOMS and AVHRR," *J. Geophys. Res.* **104**, 4037-4050 (1999) [doi:10.1029/1998JD200073].

[18] A. Bonfiglio, M. Macchiato, N. Pergola, and C. Pietrapertosa, & V. Tramutoli, "AVHRR automated detection of volcanic clouds," *Int. J. Rem. Sens.* **26** (1), 927 (2005) [doi:10.1080/0143116042000274122].

[19] W. Rose and G.C. Mayberry, "Use of GOES thermal infrared imagery for eruption scale measurements, Soufriere Hills, Montserrat," *Geoph. Res. Lett.* **27** (19), 3097-3100 (2000) [doi:10.1029/1999GL008459].

[20] G. P. Ellrod, B. H. Connell, and D. W. Hillger, Improved detection of airborne volcanic ash using multispectral infrared satellite data, *J. Geophys. Res.* **108** (D12), 4356-4369 (2003) [doi:10.1029/2002JD002802].

[21] D. W. Hillger and J. D. Clark, "Principal component image analysis of MODIS for volcanic ash. Part I: Most Important Bands and Implications for Future GOES Imagers," *J. Appl. Meteorol.* **41** (10), 985-1001 (2002) [doi:10.1175/1520-0450(2002)041<1003:PCIAOM>2.0.CO;2].

[22] I. M. Watson, V. J. Realmuto, W. I. Rose, A. J. Prata, G. J. S. Bluth, Y. Gu, C. E. Bader, and T. Yu, "Thermal infrared remote sensing of volcanic emissions using the moderate resolution imaging spectroradiometer," *J. Volcanol. Geoth. Res.* **135** (1-2), 75-89 15 July (2004) [doi:10.1016/j.jvolgeores.2003.12.017].

[23] A. Tupper, S. Carn, J. Davey, Y. Kamada, R. Potts, and F. Prata, "An evaluation of volcanic cloud detection techniques during recent significant eruption in the western Ring of Fire," *Rem. Sens. Environ.* **91**, 2746 (2004) [doi:10.1016/j.rse.2004.02.004].

[24] A. Berk, L. S. Bernstein, and D. C. Robertson, "MODTRAN: A Moderate Resolution Model for LOWTRAN7," *Rep. GL-TR-89-0122* Air Force Geophys. Lab., Bedford, MA (1989).

[25] G. P. Anderson, F. X. Kneizys, J. H. Chetwynd, J. Wang, M. L. Hoke, L. S. Rithman, L. M. Kimball, R. A. McClatchey, E. P. Shettle., S. A. Clought, W. O. Gallery, L. W. Abreu, and J. E. A. Selby, "FASCODE/MODTRAN/LOWTRAN: Past/Present/Future", *18th Annual Review Conference on Atmospheric Transmission Models*, 6-8 June (1995).

[26] W. L. Barnes, T. S. Pagano, and V. V. Salomonson, "Prelaunch characteristics of the Moderate Resolution Imaging Spectroradiometer (MODIS) on EOS-AM1," *IEEE Trans. Geosci. Rem. Sens.* **36** (4), 1088-1100 (1998) [doi:10.1109/36.700993].

[27] "MODIS home page", http://modis.gsfc.nasa.gov/

[28] P. Allard, J. Carbonelle, D. Dajlevic, J. Le Bronec, P. Morel, M.C. Robe, J.M. Maurenas, R.F. Pierret, D. Martins, J.C. Sabroux, and P. Zettwoog, "Eruptive and diffuse emission of CO_2 from Mount Etna," *Nature* **351**, 387 (1991) [doi:10.1038/351387a0].

[29] D. Andronico, S. Branca, S. Calvari, M. Burton, T. Caltabiano, R. A. Corsaro, P. Del Carlo, G. Garfi, L. Lodato, L. Miraglia, F. Mur, M. Neri, E. Pecora, M. Pompilio, G. Salerno, and L. Spampinato, "A multi-disciplinary study of the 2002-03 Etna eruption: insights into a complex plumbing system," *Bull. Volcanol.* **67** 314-330 (2005) [doi:10.1007/s00445-004-0372-8].

[30] C. Spinetti, M.F. Buongiorno, F. Doumaz , M. Musacchio, V. Lombardo, A. Harris, A. Steffke, and S. Amici, "Rapporto eruzione Etna 21-24 Novembre 2006," (Nov. 24, 2006) http://www.ct.ingv.it/Report/RPTVG200611224Roma.pdf.

[31] E. De Beni, G. Norini, and M. Polacci, "Aggiornamento dellattivit eruttiva (24 Novembre 2006, ore 13:00)," (Nov. 24, 2006) http://www.ct.ingv.it/Report/ RPTVGALT20061124_1300.pdf

[32] B. Behncke and M. Neri, "The July-August 2001 eruption of Mt. Etna (Sicily)," *Bull. Volcanol.* **65** 461-476, (2003) [doi:1010.1007/s00445-004-0372-8].

[33] C. Spinetti, D. Andronico, J. Taddeucci, A. Cristaldi, and M. F. Buongiorno, "Ash plumes at MT. Etna during the 2006 eruption: observations from satellite to microscope," presented at *24^{th} IUGG Conference*, 2-13 July 2007, Perugia (Italy), Poster Session **VS015**.

[34] G. C. Mayberry, W. I. Rose, and G. J. S. Bluth, "Dinamics of the volcanic and meteorological clouds produced by the December 26, 1997 eruption of Soufriere Hills volcano, Montserrat, 1995-99," edited by T. Druitt and P. Kokelaar, *Mem. Geol. Soc. Lond.* **21**, 539-555 (2002).

[35] S. Pugnaghi, S. Teggi, S. Corradini, M. F. Buongiorno, M. P. Bogliolo, and L. Merucci, "Estimation of SO_2 abundance in the eruptive plume of Mt. Etna using two MIVIS thermal infrared channels: a case study from the Sicily-1997 campaign," *Bull. Volcanol.* **64** 328-337 (2002) [doi:10.1007/s00445-002-0211-8].

[36] S. Corradini, S. Pugnaghi, S. Teggi, M. F. Buongiorno, and M. P. Bogliolo, Will ASTER see the Etna SO2 plume?, *Int. J. Rem. Sens.* **24** (6), 12071218 (2003) [doi:10.1080/01431160210153084].

[37] S. Pugnaghi, G. Gangale, S. Corradini, and M. F. Buongiorno, "Mt. Etna sulfur dioxide flux monitoring using ASTER-TIR data and atmospheric observations," *J. Volcanol. Geoth. Res.* **152** 7490 (2006) [doi:10.1016/j.jvolgeores.2005.10.004].

[38] Oxford University, Atmospheric Oceanic and Planetary Physics Dept., EODG group Mie Code, "Light scattering routines," (2006) http://www.atm.ox.ac.uk/code/mie/index.html.

[39] F. E. Volz, "Infrared optical constants of ammonium sulfate, Sahara dust, volcanic pumice and fly ash," *Appl. Optic.* **12** 564-568 (1973).

[40] "NASA emissivities database," http://speclib.jpl.nasa.gov/

[41] J. B. Pollack, O. B. Toon, and B. N. Khare, "Optical properties of some terrestrial rocks and glasses", *Proc. Icarus* **19** 372-389 (1973) [doi:10.1016/0019-1035(73)90115-2].

[42] G. Gangale, "Controllo del flusso di SO_2 dell'Etna utilizzando dati ASTER e profili atmosferici," *Degree Thesis*, Univ. Modena and Reggio Emilia (2005).